Field-effect control of single-molecule, carbon-based thermoelectric nanodevices

Pascal Gehring,[1]* Jean Spièce,[2] Achim Harzheim,[1] Yuewen Sheng,[1]
Gregory Rogers,[1] Aadarsh Mishra,[1] Benjamin Robinson,[2,3]
Kyriakos Porfyrakis,[1] Jamie H. Warner,[1] Oleg Kolosov,[2]
G. Andrew. D. Briggs,[1] Jan A. Mol[1]

[1]Department of Materials, University of Oxford, 16 Parks Road, Oxford OX1 3PH, UK
[2]Physics Department, Lancaster University, Lancaster LA1 4YB, UK
[3]Materials Science Institute, Lancaster University, Lancaster, LA1 4YW, UK

*To whom correspondence should be addressed; E-mail: pascal.gehring@materials.ox.ac.uk.

Organic thermoelectric materials could potentially provide an energy-efficient route towards low-cost waste heat recovery. A key strategy for improving the thermoelectric performance of inorganic materials has been to take advantage of nanostructuring which leads to quantum confinement of electrons and suppression of parasitic phonons[1, 2]. A similar enhancement of the conversion efficiency is to be expected in nanostructured organic materials[3]. Although it was demonstrated that discrete molecular levels determine the sign and magnitude of thermopower in single-molecule junctions[4, 5, 6], full electrostatic control of these levels has not been achieved to date. Here, we show that graphene nanogaps combined with gold micro-heaters serve as a testbed for studying single-molecule thermoelectricity. Reduced screening of the gate electric field allows optimisation of the thermopower by controlling the position of the dominant transport orbital relative to the chemical potential of the electrodes. We find that the power factor

of a graphene-fullerene junction can be tuned over a range of five orders of magnitude to a value close to the theoretical limit. These results open up new avenues for exploring thermopower and charge transport in individual molecules, and highlight the importance of level-alignment to achieve the optimum energy conversion in organic thermoelectric materials.

The thermopower or Seebeck coefficient S of a material or nanoscale device is defined as $S = -\Delta V/\Delta T$, where ΔV is the voltage difference generated between the two ends of the junction when a temperature difference ΔT is established between them. In addition to the goal of maximising S, there is a great demand for materials with a high power factor $S^2 G$ and high thermoelectric efficiency, which is expressed in terms of a dimensionless figure of merit $ZT = S^2 GT/\kappa$, where T is the average temperature, G is the electrical conductance and κ is the sum of the electronic and phononic contribution to the thermal conductance. In conventional thermoelectric materials S, G and κ are typically mutually contra-indicated, such that high S is accompanied by low G and high G by high κ[7]. In nanostructured materials these properties can be decoupled[1]. Values of $ZT \sim 2$ were realised in for example PbSeTe/PbTe-based quantum dot superlattices where the transport is dominated by one level with a sharp transmission function[8]. Organic nanostructured materials could be flexible, cheap, environmentally friendly, and potentially have even higher thermoelectric efficiencies. Moreover, the single-molecule building blocks of organic materials offer energy-level spacings which are orders of magnitude greater than $k_\text{B}T$ at room temperature. The ability to measure thermopower in single-molecule junctions is relatively new and the thermoelectric properties of only a few molecules have been measured[6, 9, 4, 10, 11, 12, 5, 13]. In the past few years it has been demonstrated both experimentally and theoretically that, at the molecular scale, S can be controlled by varying the chemical composition[10], by varying the position of intra-molecular energy levels relative to the work function of metallic electrodes[12], by systematically increasing

2

the single-molecule lengths within a family of molecules[4, 11], and by tuning the interaction between two neighbouring molecules.[9] Despite these advances, single-molecule experiments have only yielded values of S ranging from 1 to 50 μV K^{-1}[6, 14]. The key challenge in achieving high thermopower lies in controlling the transport resonances in molecular junctions.

The two-dimensional nature of graphene electrodes reduces the screening of the gate electric field compared to metal electrodes[15]. As a result, orbital energy levels can be tuned over a wide range in graphene-based single-molecule devices. We exploit this field-effect control to map the thermopower across entire molecular transport resonances. Our devices consist of CVD graphene etched into bow-tie shape on-top of gold contacts (see Methods for fabrication details). Each gold lead has four contacts for precise 4-terminal resistance measurements, which enable us to measure the temperature difference across the graphene junction (see Figure S1 Supplementary Information). A gold micro-heater is located 1 μm away from the junction (see Figure 1a). By passing a current through the micro-heater we create a temperature gradient along the sample[16, 17, 18]. We quantify the temperature gradient across the graphene junction by: (i) measuring the resistance of the left and right gold contacts; (ii) using COMSOL finite-element simulations; and (iii) using Scanning Thermal Microscopy (SThM) measurements. Using method (i) we measure a temperature difference between the left and right contact as a function of heater power $\Delta T/P_{\text{heater}} = 43$ K W^{-1} $\pm xxx$ at $T_0 = 77$ K. This is in close agreement with the finite-element simulations which predict $\Delta T/P_{\text{heater}} = 50$ K W^{-1} and a constant temperature gradient $\nabla T/P_{\text{heater}} = 14$ K μm^{-1} W^{-1} across the length of the graphene junction (see Figure S3). Figure 1b shows a temperature map overlaid onto a height profile that were simultaneously recorded using a SThM. From the temperature maps recorded for different heater powers in Figure 1c and d we extract a power-dependent temperature gradient $\nabla T/P_{\text{heater}} = 18$ K μm^{-1} W^{-1} and a temperature difference $\Delta T/P_{\text{heater}} = 63 \pm 10$ K W^{-1} between the two gold contacts.
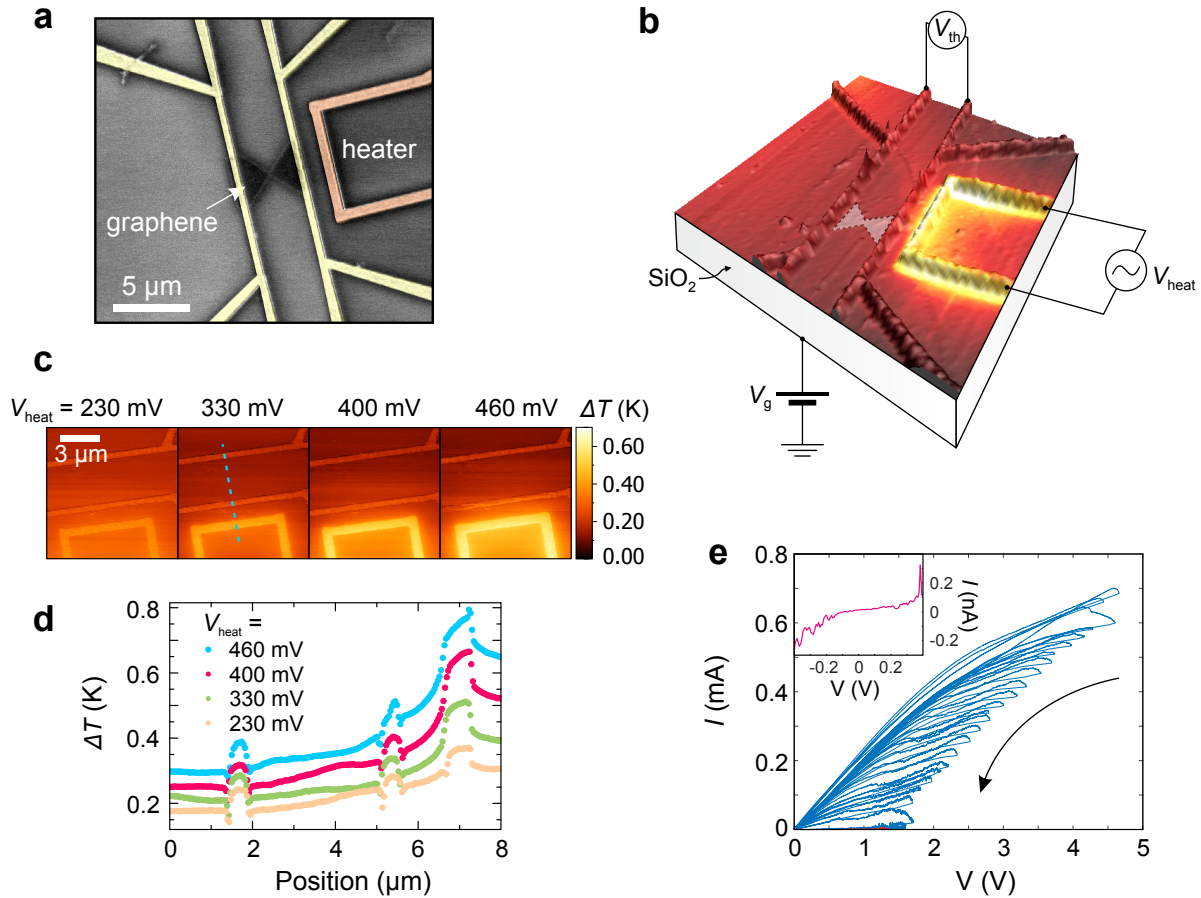
Figure 1: **Device geometry and Scanning Thermal Microscopy.** **a**, False-colour scanning electron microscopy image of the device. **b**, Atomic force microscopy height profile overlaid with scanning thermal microscopy signal and sketch of the device geometry for a typical thermopower measurement. **c**, Scanning thermal microscopy images recorded at different constant voltages V_{heat} applied to the micro-heater. **d**, Line profiles along the device extracted from the maps shown in **c** (see blue dotted line). **e**, IV_{sd} traces recorded during feedback-controlled electroburning. Inset: IV_{sd} trace after completed electroburning.

We use feedback-controlled electroburning[19, 20] (see Figure 1e) to form graphene nanoconstrictions showing quantum interference effects[21], graphene quantum dots showing sequential tunnelling[22] and empty gaps suitable for characterisation of single molecules[23, 24]. We first perform a baseline measurement of an electroburnt graphene device without depositing molecules (Device A). The current-voltage characteristic at room temperature after elec-

⁷¹ troburning of a graphene quantum dot is shown in Figure 1e (inset), and a full conductance map

⁷² as a function of bias and gate voltage (stability diagram) at $T_0 = 20$ mK is shown in Figure

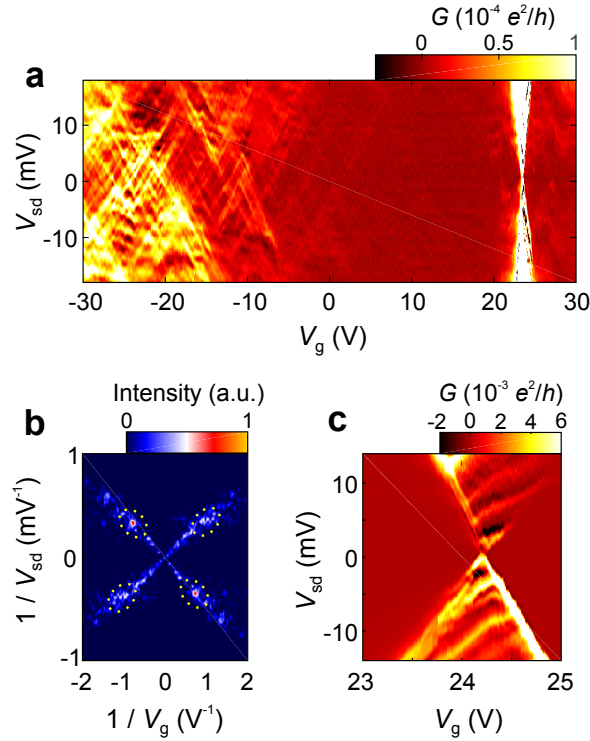2a. The transport in Device A can be tuned from the quantum interference region at negative

Figure 2: **Low-temperature transport characterisation of a graphene quantum dot (Device A). a**, Conductance map as a function of source-drain voltage V_{sd} and back gate voltage V_g measured at $T_0 = 20$ mK. **b**, Fast-Fourier-Transform of the interference regime between -30 V $> V_g > -10$ V in **a**. **c**, Close-up of the sequential tunnelling regime in **a**.

⁷³

⁷⁴ gate voltages to the sequential tunnelling region at positive gate voltages. Similar behaviour

⁷⁵ was observed before, where Coulomb blockade is typically found around the Dirac point (30

⁷⁶ - 40 V in our case) and quantum interference effects occur in highly electron or hole doped

⁷⁷ regions[25, 21]. The origin of quantum interference can be non-periodic universal conductance

⁷⁸ fluctuations (UCFs)[26, 27] or quasi-periodic single-/multimode Fabry-Pérot interferences[28].

⁷⁹ To distinguish the two effects, fast Fourier transforms (FFTs) of the chessboard pattern were

calculated and are shown in Figure 2b. We observe points of high intensity in the 2D FFT around $1/V_{\text{sd}} = 0.35$ mV^{-1}, indicated by the dotted ovals, which corresponds to a hidden periodicity in energy of about 1.4 meV. This points towards quasi-periodic multimode Fabry-Pérot interferences on a length scale of about $L = h v_{\text{F}}/(2E) = 1.2$ μm due to reflections between gold contacts and potential steps formed inside the channel during electroburning[21].

Figure 2c shows a close-up of the charge degeneracy point of the Coulomb diamond at $V_{\text{g}} = 24$ V. Many excited state lines with a slope different from the edges of the Coulomb diamond and regions of negative differential conductance can be observed inside the sequential tunnelling regime. These can be attributed to density of states fluctuations (UCFs or Fabry-Pérot, see above) in the graphene leads[29] which are mapped by the sharp transport resonance of the quantum dot.

We next investigate the thermoelectric response of Device A by separately studying the response of the interference and the sequential tunnelling region (see gate trace in Figure 3a). Figure 3b and c show the Seebeck coefficient $S = -V_{\text{th}}/\Delta T$ as a function of back gate voltage V_{g} for these two regimes, measured at constant heater voltage. The thermo-voltage V_{th} is measured at a lock-in frequency $2f$, where f is the modulation frequency of the heat voltage. S changes sign and oscillates around zero every time a conductance peak crosses the Fermi level of the electrodes. Similar thermopower oscillations were observed in graphene devices showing universal conductance fluctuations[17], in chaotic quantum dots[30], in carbon nanotubes[16] and in various semiconductor quantum dot systems[31, 32] in the sequential tunnelling regime.

When a temperature bias is applied to a junction, the Fermi-Dirac distribution $f_{\text{H}}(E)$ of the hot contact broadens compared to $f_{\text{C}}(E)$ of the cold contact (see Figure 3d and e). This gives rise to a thermal current, which can be estimated using the Landauer-Buettiker formalism[14]:

$$I_{\text{sd}} = \frac{2e}{h} \int [f_{\text{H}}(E) - f_{\text{C}}(E)]\mathcal{T}(E)\mathrm{d}E \tag{1}$$
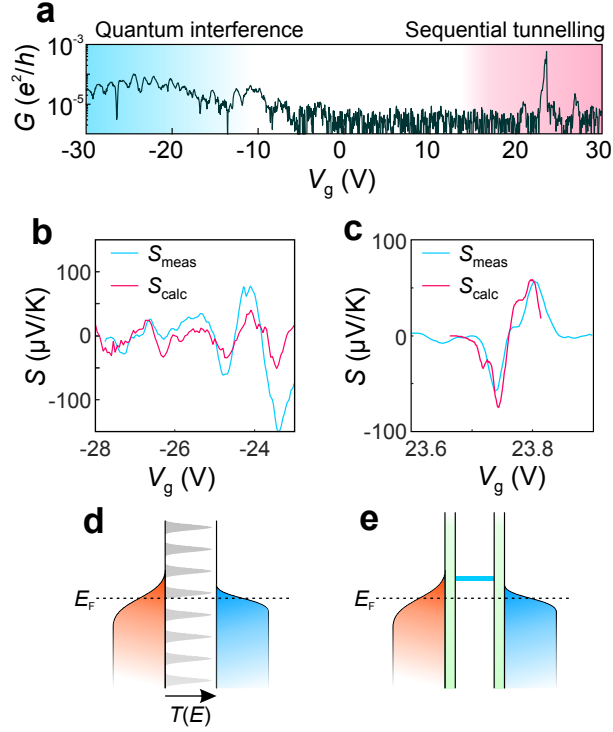
Figure 3: **Thermoelectric measurements on a graphene nanostructure. a**, Zero bias conductance trace of the data shown in Figure 2a. The quantum interference and sequential tunnelling regime are shaded blue and red, respectively. **b**, The measured and calculated Seebeck coefficient using equation 2 for the quantum interference ($\Delta T = 63$ mK) and **c**, sequential tunnelling ($\Delta T = 40$ mK) regime. **d**, Schematic representation of the electron distribution of the hot (red) and the cold (blue) lead and the density of states of the nanostructure (grey) for the quantum interference and **e**, the sequential tunnelling regime.

where $\mathcal{T}(E)$ is the transmission probability through the junction, e is the elementary charge and h is Planck's constant. This current leads to a thermo-voltage V_{th} when measured under open circuit conditions $I(\Delta T, V_{\text{th}}) = 0$. The Seebeck coefficient can also be directly obtained from the conductance data by the widely used Mott approximation[33]

$$S = -\frac{\pi^2 k_{\text{B}}^2 T_0}{3e\alpha} \frac{1}{G} \frac{\text{d}G}{\text{d}V_{\text{g}}}, \tag{2}$$

where $\alpha = \frac{\text{d}E}{\text{d}V_{\text{g}}}$ is the lever arm of the back gate and k_{B} is the Boltzmann constant. We can extract $\alpha = 8.6$ meV V^{-1} from the slopes of the Coulomb diamond in Figure 2c[34]. The pink curves in

Figure 3 b and c show the calculated Seebeck coefficients using equation 2 and the conductance data recorded at $T_0 = 350$ mK. Good agreement between the measured and calculated data is found in the sequential tunnelling regime. However, in the quantum interference region the measured thermopower is slightly larger than the value estimated using the Mott formula. This is not accounted for by the lower gate coupling $\alpha \approx 1$ meV V^{-1} in the interference regime compared to the sequential tunnelling regime. We attribute this discrepancy to the finite bias window the data was smoothed over necessary for the calculation of the numerical differential conductance.

In order to achieve good agreement between the calculated and measured Seebeck coefficients in Figure 3c we need to assume the temperature difference ΔT between the hot and the cold electrode to be equal to the temperature difference measured between the two gold contacts. This implies that hot electrons injected from the gold contacts into the graphene leads do not thermalise until they reach the quantum dot area approximately 1.7 μm away from the gold contacts and transport must therefore be ballistic. Ballistic transport over several μm has been already observed in exfoliated[35] and CVD graphene devices[36] and results in a much greater temperature drop across graphene nanoconstriction or molecular junction than expected from the temperature gradient measured using SThM. The highly energy-dependent transmission function of nanostructures can lead to a strong non-linear thermoelectric response in the regime where the thermal bias becomes bigger than the sample temperature ($\Delta T >> T_0$)[37]. This was theoretically investigated for resonant tunnelling structures[38], quantum dots[39] and experimentally investigated in quantum dots defined in heterostructured semiconductor nanowires[39, 32]. Figure 4a and b show the thermovoltage V_{th} as a function of heater voltage V_{heat} for the sequential tunnelling and interference regime, respectively. The thermovoltage increases approximately linearly in intensity with increasing ΔT. The peaks broaden in gate voltage. That can be understood in terms of the broadening of the Fermi-Dirac distributions
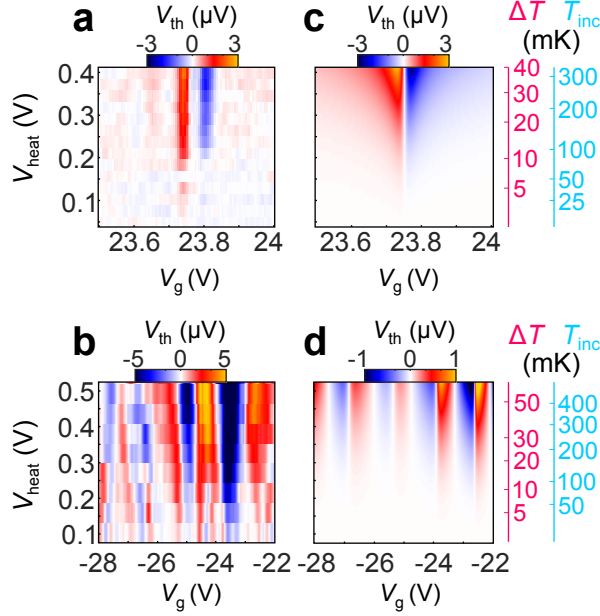
Figure 4: **Non-linear thermoelectric response. a**, Thermovoltage as a function of back gate voltage V_g and heater voltage V_{heat} for the sequential tunnelling and **b** the quantum interference regime. **c**, Simulated thermovoltage using equation 1 as a function of back gate and heater voltage for the sequential tunnelling and **d** the quantum interference regime.

$f_i(E) = 1 + \exp[(E - \mu_i)/(k_B T_i)]$ of the hot ($i = H$) and cold ($i = C$) lead[39]. We model our data using equation 1 where we assume that the micro-heater increases the temperatures T_H and T_C by different amounts, resulting in a temperature difference $\Delta T = T_H - T_C$ across the device as well as an increase of the average temperature of the nanostructure by $T_{inc} = (T_H + T_C)/2 - T_0$. We have used the values from our calibration measurements (see Figure S1 Supplementary Information) to calculate $T_H(V_{heat})$ and $T_C(V_{heat})$. The transmission function $\mathcal{T}(E)$ was extracted from the conductance data by assuming that at low temperature $G \approx e^2/h\mathcal{T}(E)$ and by fitting the data to one (sequential tunnelling regime, see Figure S4) or several (interference regime) Breit-Wigner resonances $\mathcal{T}(E) = \Gamma_H \Gamma_C/[(\mu_{QD} - E)^2 + (\Gamma_H/2 + \Gamma_C/2)^2]$, where μ_{QD} is the electrochemical potential of the quantum dot and where we define the tunnel coupling Γ_i of the hot ($i = H$) and cold ($i = C$) lead as $\Gamma_i = \hbar\frac{1}{\tau_i}$ ($\frac{1}{\tau_i}$: tunnel rate).

9

The results of the simulation using equation 1 for the sequential tunnelling and the interference regime are shown in Figure 4 c and d, respectively. The gate voltage for which the thermovoltage changes sign varies slightly with increasing V_{heat}. Similar behaviour was observed before and has been attributed to a temperature dependent renormalisation of the resonance energies of the quantum dot[39].
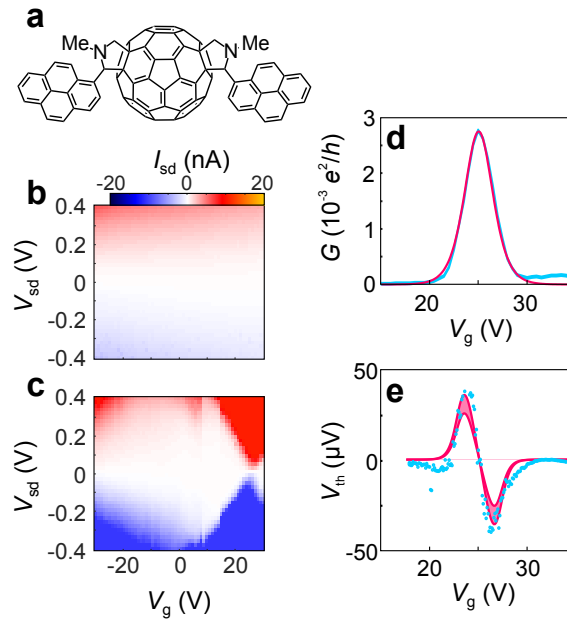

Figure 5: **Electrostatic control of the thermopower of a single C_{60} molecule. a,** Chemical structure of the C_{60} bisadducts functionalised with pyrene anchor groups. **b,** Current map as a function of back gate and bias voltage before and **c,** after molecule deposition recorded at $T_0 = 77$ K. **d,** Zero-bias conductance and **e,** Seebeck coefficient (measured at $\Delta T = 66$ mK) of the molecular junction as a function of back gate voltage measured at $T = 77$ K. **f,** Seebeck coefficient as a function of back gate and heater voltage measured at $T_0 = 77$ K.

After having determined that the thermoelectric properties of graphene nanostructure devices are well described by the existing theory we will address the question: can a single-molecule junction outperform a conventional quantum dot? To this end we have fabricated graphene nano-gaps using feedback controlled electroburning and coupled C_{60} molecules functionalised with pyrene anchor groups (see Figure 5a) to the graphene leads. This molecule

serves as a benchmark for single-molecule thermoelectric studies since it has been successfully coupled to graphene electrodes[24] and its thermoelectric properties have been studied using various techniques, including STM based break junctions[12, 9] and electromigrated gold break junctions[6]. We identify empty graphene gaps by measuring the current I_{sd} as a function of gate and bias voltage at $T_0 = 77$ K under vacuum. Empty devices are characterised by non-linear tunnelling $I_{sd} - V_{sd}$ curves and little or no gate modulation. After pre-characterisation we warm up the device and deposit C_{60} molecules by immersing the sample in a 10 μM chloroform solution containing the C_{60} bisadducts for 1 min followed by blow drying with nitrogen gas. Figure 5b and c show the stability diagrams of the same device (Device B) measured at 77 K before and after molecule deposition. The formation of a molecular junction results in a conductance peak at $V_g = 25$ V in the stability diagram (see Figure 5c and d)[19, 24, 23]. The full width half maximum (FWHM) of the conductance peak is 22 meV which is very close to the theoretical value of $\approx 3.3k_BT$ for a thermally broadened conductance peak. Thus we conclude that at $T_0 = 77$ K the quantum dot is in the weak-coupling regime ($\Gamma \ll k_BT$). Consequently, we can only use the amplitude of the conductance peak to estimate the tunnel coupling where we assume symmetric coupling ($\Gamma_L = \Gamma_R$) to reduce the number of variables. To this end we can estimate $\Gamma = \Gamma_L + \Gamma_R$, α and the energy E_0 of the transport resonance by fitting the data with a thermally broadened conductance peak $G = \frac{\pi e^2}{2h}\Gamma\frac{1}{4k_BT}\cosh^{-2}\left[(\alpha V_g - E_0)/(2k_BT_0)\right]$ where we fix $T_0 = 77$ K and obtain $\Gamma = xxx$ μeV, $\alpha = 9$ meV V^{-1} and $E_0 = 221$ meV, respectively. Next, we measure the gate dependent thermopower of a single C_{60} molecule. We focus on the region of high conductance around $V_g = 25$ V (see gate trace in Figure 5d). Figure 5e shows the Seebeck coefficient as a function of back gate voltage recorded at $V_{heat} = 400$ mV, which corresponds to a temperature difference $\Delta T = 66$ mK between the left and right contact. A decrease of S followed by a sign change, further increase and subsequent decrease towards zero can be observed. We find a maximum thermopower of $S_{max} = 0.6\pm0.1$ mV K^{-1} which is nearly

11

constant up to a temperature bias of $\sim$70 mK (see Figure 5f). This value is more than one order of magnitude larger than the Seebeck coefficients found in STM break junction experiments of C_{60} contacted with different metal electrodes[12, 9].

Using this result we can estimate the maximum power factor S^2G which can be tuned by more than five orders of magnitude by electrical gating to a maximum value of $0.07\times k_\mathrm{B}^2/h$ (see Figure S6 Supplementary Information). We can compare this to the maximum value of the function

$$S^2G = \frac{2}{hT_0^2}\frac{L_1^2}{L_0},\tag{3}$$

where $L_i = \int_{-\infty}^{\infty} (E - E_\mathrm{F})^i \; P(E) \, dE$ are the moments of the transmission coefficient $P(E) = -\mathcal{T}(E)\frac{\partial f(E)}{\partial E}$, $\mathcal{T}(E)$ is the transmission probability, E_F is the Fermi energy and $f(E)$ is the Fermi-Dirac distribution at T_0. We find that the power factor of our devices is very close to the maximum value of $S^2G \approx \frac{1}{2.2} \times k_\mathrm{B}^2/h$ at $h\Gamma \approx 1.1\; k_B T_0$ for a thermally and lifetime broadened transport resonance, where we assume $\mathcal{T}(E)$ to be a Breit-Wigner resonance (see Section S7 Supplementary Information). In addition, this value is about one to two orders of magnitude larger than values found in C_{60} junctions without sufficient electric field control[12, 9, 13] and comparable to $0.17\times k_\mathrm{B}^2/h$ found for C_{60} measured at 100 K using gold break junctions with an electrical back gate[6].

Thus, although the thermopowers found in this study are much higher than the values reported by others the power factors are comparable. The reason is that the tunnel coupling influences conductance and Seebeck coefficient oppositionally: increasing the coupling, like in the case of gold break junctions, will increase the conductance but decrease the Seebeck coefficient and vice versa. In the case of graphene electrodes we find a weak coupling strength of about 266 μeV, which is about a factor of 27 smaller than the optimum value of 7 meV for operation at 77 K. On the other hand, the coupling strength for C_{60} contacted with Au electrodes was estimated to be 32 meV which is about a factor of 4 larger than the ideal value for 100 K.

To achieve a maximum power factor the tunnel coupling needs to be precisely controlled to its optimum value of about $h\Gamma \approx 1.1\ k_B T_0$ by molecular design. Based on these results we conclude that, when the charge transport is dominated by a single molecular level, the thermo-electric properties of individual molecules and semiconductor quantum dots are identical. This will apply when the molecule exhibits a Breit-Wigner resonance but might change if a different quantum interference effect such as a Fano resonance is introduced[40].

We have fabricated a graphene based thermoelectric device in which a single fullerene molecule is anchored between source and drain leads. We demonstrate that by applying a thermal bias across the junction we can measure a gate dependent thermoelectricity. Our results show that by carefully tuning the transmission of a molecular junction towards sharp isolated resonance features, extremely high power factors can be achieved approaching the theoretical limit of a thermally and lifetime broadened Coulomb peak. These results are relevant for the development of organic thermoelectric materials and our approach could also be applied to test hypotheses about the thermoelectric properties of molecules exhibiting quantum interference effects[41] and spin caloritronics[42].

Methods

Device fabrication

Our devices are fabricated from single-layer CVD-grown graphene, which we transfer onto a Si/300 nm SiO$_2$ wafer with prepatterned 10 nm Cr/70 nm Au contacts and microheater. We pattern the graphene into a bowtie shape (see Figure 1a) using standard electron beam lithography and O$_2$ plasma etching. The channel length L of the devices and the width W of the narrowest part of the constriction are 3.5 μm and 200 nm, respectively. To narrow down the constriction or form a nanogap we use a feedback-controlled electroburning technique in air[21] using a ADWin Gold II card with a 30 kHz sampling rate. Electroburning cycles are repeated until a

critical resistance of 500 MΩ is reached.

Scanning thermal microscopy temperature measurements

These were performed in ambient environment using a commercial SPM (BrukerMultiMode with Nanoscope E controller) and a custom-built SThM modified AC Wheatstone bridge. A resistive SThM probe (Kelvin Nanotechnology, KNT-SThM-01a, 0.3 N/m springconstant, < 100 nm tip radius) served as one of the bridge resistors allowing precise monitoring of the probe AC electrical resistance at 91 kHz frequency via lock-in detection of the signal (SRS Instruments, SR830) as explained elsewhere[43]. Surface temperature maps were obtained at varying DC current to the probe that generated variable Joule heating of the probe tip. Several driving currents were used ranging from 0.10 to 0.40 mA leading to excess probe temperatures up to 34 K. The probe temperature electrical resistance relation was determined using a calibrated Peltier hot/cold plate (Torrey Pines Scientific, Echo Therm IC20) using a ratiometric approach (Agilent 34401A)[43]. The double-scan technique was used with different probe driving currents in order to obtain quantitative measurements of the surrounding and of the heater temperature[44]. Laser illumination on the probe (on the order of 5 K) added to the Joule heating and was accounted via measurement of corresponding probe resistance change. SThM thermal mapping was performed with a set-force below 15 nN during imaging to protect the tip and the sample from damage.

Electric and thermoelectric transport measurements

Graphene nano-structures were characterised in an Oxford Instruments Triton 200 dilution refrigerator with 20 mK base temperature. All measurements on C_{60} junctions were performed in a liquid nitrogen dip-stick setup. Electrical DC transport measurements were performed using low-noise DC electronics (Delft box). To measure the thermoelectric properties of nano-

254 structures we used the $2f$ method[16]. To this end an AC heater voltage $V_{\text{heat}}(f)$ with frequency

255 f was applied to the micro-heater using a HP33120a arbitrary waveform generator. The ther-

256 movoltage was measured with a SRS830 lock-in amplifier at a frequency $2f$.

References and Notes

[1] Venkatasubramanian, R., Siivola, E., Colpitts, T. & O'Quinn, B. Thin-film thermoelectric devices with high room-temperature figures of merit. *Nature* **413**, 597–602 (2001). URL http://dx.doi.org/10.1038/35098012. 10.1038/35098012.

[2] Karlstrom, O., Linke, H., Karlstrom, G. & Wacker, A. Increasing thermoelectric performance using coherent transport. *Physical Review B* **84**, 113415 (2011).

[3] Murphy, P., Mukerjee, S. & Moore, J. Optimal thermoelectric figure of merit of a molecular junction. *Phys. Rev. B* **78**, 161406 (2008). URL http://link.aps.org/doi/10.1103/PhysRevB.78.161406.

[4] Reddy, P., Jang, S.-Y., Segalman, R. A. & Majumdar, A. Thermoelectricity in molecular junctions. *Science* **315**, 1568–1571 (2007). URL http://science.sciencemag.org/content/315/5818/1568. http://science.sciencemag.org/content/315/5818/1568.full.pdf.

[5] Widawsky, J. R., Darancet, P., Neaton, J. B. & Venkataraman, L. Simultaneous determination of conductance and thermopower of single molecule junctions. *Nano Letters* **12**, 354–358 (2012). URL http://dx.doi.org/10.1021/nl203634m. PMID: 22128800, http://dx.doi.org/10.1021/nl203634m.

[6] Kim, Y., Jeong, W., Kim, K., Lee, W. & Reddy, P. Electrostatic control of thermoelectricity in molecular junctions. *Nature Nanotechnology* **9**, 881–885 (2014). URL http://dx.doi.org/10.1038/nnano.2014.209.

[7] Heremans, J. P., Dresselhaus, M. S., Bell, L. E. & Morelli, D. T. When thermoelectrics reached the nanoscale. *Nat Nano* **8**, 471–473 (2013). URL http://dx.doi.org/10.1038/nnano.2013.129.

[8] Harman, T. C., Taylor, P. J., Walsh, M. P. & LaForge, B. E. Quantum dot superlattice thermoelectric materials and devices. *Science* **297**, 2229–2232 (2002). URL http://science.sciencemag.org/content/297/5590/2229. http://science.sciencemag.org/content/297/5590/2229.full.pdf.

[9] Evangeli, C. *et al.* Engineering the Thermopower of C 60 Molecular Junctions. *Nano Letters* **13**, 2141–2145 (2013).

[10] Baheti, K. *et al.* Probing the chemistry of molecular heterojunctions using thermoelectricity. *Nano Letters* **8**, 715–719 (2008). URL http://dx.doi.org/10.1021/nl072738l. PMID: 18269258, http://dx.doi.org/10.1021/nl072738l.

[11] Malen, J. A. *et al.* The nature of transport variations in molecular heterojunction electronics. *Nano Letters* **9**, 3406–3412 (2009). URL http://dx.doi.org/10.1021/nl9013875. PMID: 19711966, http://dx.doi.org/10.1021/nl9013875.

[12] Yee, S. K., Malen, J. A., Majumdar, A. & Segalman, R. A. Thermoelectricity in Fullerene À Metal Heterojunctions. *Nano Letters* **11**, 4089–4094 (2011).

16

[13] Rincon-Garcia, L. *et al.* Molecular design and control of fullerene-based bi-thermoelectric materials. *Nat Mater* **15**, 289–293 (2016). URL http://dx.doi.org/10.1038/nmat4487.

[14] Rincon-Garcia, L., Evangeli, C., Rubio-Bollinger, G. & Agrait, N. Thermopower measurements in molecular junctions. *Chem. Soc. Rev.* **45**, 4285–4306 (2016). URL http://dx.doi.org/10.1039/C6CS00141F.

[15] Lortscher, E. Wiring molecules into circuits. *Nat Nano* **8**, 381–384 (2013). URL http://dx.doi.org/10.1038/nnano.2013.105.

[16] Small, J. P., Perez, K. M. & Kim, P. Modulation of Thermoelectric Power of Individual Carbon Nanotubes. *Physical Review Letters* **91**, 256801 (2003).

[17] Zuev, Y. M., Chang, W. & Kim, P. Thermoelectric and Magnetothermoelectric Transport Measurements of Graphene. *Physical Review Letters* **096807**, 1–4 (2009).

[18] Devender *et al.* Harnessing Topological Band Effects in Bismuth Telluride Selenide for Large Enhancements in Thermoelectric Properties through Isovalent Doping. *Advanced Materials* **28**, 6436–6441 (2016). URL http://onlinelibrary.wiley.com/doi/10.1002/adma.201601256/full.

[19] Prins, F. *et al.* Room-Temperature Gating of Molecular Junctions Using Few-Layer Graphene Nanogap Electrodes. *Nano Letters* **11**, 4607–4611 (2011).

[20] Lau, C. S., Mol, J. A., Warner, J. H. & Briggs, G. A. D. Nanoscale control of graphene electrodes. *Phys. Chem. Chem. Phys.* **16**, 20398–20401 (2014). URL http://dx.doi.org/10.1039/C4CP03257H.

17

[21] Gehring, P. *et al.* Quantum Interference in Graphene Nanoconstrictions. *Nano Letters* **16**, 4210–4216 (2016).

[22] Puczkarski, P. *et al.* Three-terminal graphene single-electron transistor fabricated using feedback-controlled electroburning. *Applied Physics Letters* **107** (2015). URL `http://scitation.aip.org/content/aip/journal/apl/107/13/10.1063/1.49321`

[23] Mol, J. A. *et al.* Graphene-porphyrin single-molecule transistors. *Nanoscale* **7**, 13181–13185 (2015). URL `http://dx.doi.org/10.1039/C5NR03294F`.

[24] Lau, C. S. *et al.* Redox-Dependent Franck Condon Blockade and Avalanche Transport in a Graphene Fullerene Single-Molecule Transistor. *Nano Letters* **16**, 170–176 (2016). URL `http://pubs.acs.org/doi/pdf/10.1021/acs.nanolett.5b03434`.

[25] Bischoff, D., Libisch, F., Burgd, J., Ihn, T. & Ensslin, K. Characterizing wave functions in graphene nanodevices : Electronic transport through ultrashort graphene constrictions on a boron nitride substrate. *Physical Review B* **90**, 115405 (2014).

[26] Lee, P. A., Stone, A. D. & Fukuyama, H. Universal conductance fluctuations in metals: Effects of finite temperature, interactions, and magnetic field. *Physical Review B* **35**, 1039 (1987).

[27] Morozov, S. V. *et al.* Strong Suppression of Weak Localization in Graphene. *Physical Review Letters* **97**, 016801 (2006).

[28] Oksanen, M. *et al.* Single-mode and multimode Fabry-Perot interference in suspended graphene. *Physical Review B* **89**, 121414 (2014).

[29] Gehring, P. *et al.* Disentangling lead and molecule states in graphene-based single-electron transistors (submitted) (2016).

[30] Godijn, S. F., Möller, S., Buhmann, H. & Molenkamp, L. W. Thermopower of a Chaotic Quantum Dot. *Physical Review Letters* **82**, 2927–2930 (1999).

[31] Staring, A. A. M. *et al.* Coulomb-Blockade Oscillations in the Thermopower of a Quantum Dot . *Europhysics Letters* **22**, 57–62 (1993).

[32] Svilans, A., Burke, A. M., Leijnse, M. & Linke, H. Nonlinear thermoelectric response due to energy-dependent transport properties of a quantum dot. *Physica E* **82**, 34–38 (2016).

[33] Lunde, A. M. & Flensberg, K. On the Mott formula for the thermopower of non-interacting electrons in quantum point contacts. *JOURNAL OF PHYSICS: CONDENSED MATTER* **17**, 3879–3884 (2005).

[34] Hanson, R., Kouwenhoven, L. P., Petta, J. R., Tarucha, S.,& Vandersypen, L. M. K. Spins in few-electron quantum dots. *Reviews of Modern Physics* **79**, 1217–1265 (2007).

[35] Miao, F. *et al.* Phase-coherent transport in graphene quantum billiards. *Science* **317**, 1530–1533 (2007). URL http://science.sciencemag.org/content/317/5844/1530. http://science.sciencemag.org/content/317/5844/1530.full.pdf.

[36] Banszerus, L. *et al.* Ballistic transport exceeding 28 m in cvd grown graphene. *Nano Letters* **16**, 1387–1391 (2016). URL http://dx.doi.org/10.1021/acs.nanolett.5b04840. PMID: 26761190, http://dx.doi.org/10.1021/acs.nanolett.5b04840.

[37] Sierra, M. A. & Sanchez, D. Strongly nonlinear thermovoltage and heat dissipation in interacting quantum dots. *Physical Review B* **90**, 115313 (2014).

[38] Sanchez, D. & Lopez, R. Scattering Theory of Nonlinear Thermoelectric Transport. *Physical Review Letters* **110**, 026804 (2013).

[39] Svensson, S. F., Hoffmann, E. A. & Nakpathomkun, N. Nonlinear thermovoltage and thermocurrent in quantum dots. *New Journal of Physics* **15**, 105011 (2013). URL http://iopscience.iop.org/article/10.1088/1367-2630/15/10/105011/pdf.

[40] Lambert, C. J., Sadeghi, H. & Al-Galiby, Q. H. Quantum-interference-enhanced thermoelectricity in single molecules and molecular films. *Comptes Rendus Physique* **17**, 1084–1095 (2016).

[41] Finch, C. M. & Lambert, C. J. Giant thermopower and figure of merit in single-molecule devices. *Physical Review B* **79**, 033405 (2009). URL http://journals.aps.org/prb/pdf/10.1103/PhysRevB.79.033405.

[42] Wang, R.-Q., Sheng, L., Shen, R., Wang, B. & Xing, D. Y. Thermoelectric effect in single-molecule-magnet junctions. *Phys. Rev. Lett.* **105**, 057202 (2010). URL http://link.aps.org/doi/10.1103/PhysRevLett.105.057202.

[43] Tovee, P., Pumarol, M., Zeze, D., Kjoller, K. & Kolosov, O. Nanoscale spatial resolution probes for scanning thermal microscopy of solid state materials. *Journal of Applied Physics* **112**, 114317 (2012). URL http://scitation.aip.org/content/aip/journal/jap/112/11/10.1063/1.47679

[44] Menges, F., Riel, H., Stemmer, A. & Gotsmann, B. Quantitative thermometry of nanoscale hot spots. *Nano Letters* **12**, 596–601 (2012). URL http://dx.doi.org/10.1021/nl203169t. PMID: 22214277, http://dx.doi.org/10.1021/nl203169t.

Acknowledgements

Contributions

P.G. designed and planed the project, fabricated the devices and performed the electric and thermoelectric transport measurements. A.H. recorded supporting C_{60} data. J.S., B.R. and O.K. performed the scanning thermal microscopy measurements. P.G. and J.A.M. performed the theoretical transport calculations. A.M. performed the COMSOL simulations. G.R. and K.P. synthesised the C_{60} molecules. Y.S. and J.H.W. synthesised the CVD graphene. P.G. drafted the manuscript and all authors contributed to the final version of the manuscript. G.A.D.B. and J.A.M. supervised the project.

Competing financial interests

The authors declare no competing financial interests.